UDC 544.772:544.47:621.791

PHYSICOCHEMICAL AND CATALYTIC PROPERTIES OF THE SOLID COMPONENT OF WELDING AEROSOL

T.L. Rakitskaya [1,2]**, A.A. Ennan** [2]**, A.S. Truba** [1,2]**, S.A. Kiro** [2]**, V.Y. Volkova** [1]

[1] *Mechnickov National University of Odessa, Faculty of Chemistry*
2 Dvoryanskaya Str., Odessa, 65082, Ukraine, E-mail: truba@onu.edu.ua
[2] *Physicochemical Institute of Environment and Human Protection*
3 Preobrazhenskaya Str., Odessa, 65026, Ukraine

The samples of the solid component of aerosol produced due to steel welding with a TsL-11 type electrode (ISO E19.9NbB20) have been characterized by X-ray phase analysis, IR spectroscopy, and pH-metry. Manganochromite, oxides of iron, manganese, and nickel are the phases causing low-temperature catalytic ozone decomposition.

Keywords: *welding aerosol, solid component, characterisation, ozone decomposition, air purification*

INTRODUCTION

Atmospheric emission of welding aerosols is a result of complex physical and chemical processes taking place in the course of welding. The solid component of welding aerosol (SCWA) is the airdispersed particulate formed out of the welding arc in consequence of the oxidation and condensation of vapors of components of electrode coatings, welding fluxes, and metals. A composition of the gaseous component of welding aerosol (GCWA) depends on the nature of materials applied and welding conditions influencing the proceeding of reactions following by HF, SiF_4, CO, NO_x , and O_3 formation [1–5]. Among the listed gases, ozone is an extremely hazardous compound with maximum permissible concentration (MPC) within working areas of only 0.1 mg/m^3. Taking into account the extent of welding and related fabrications as well as the variety of welding techniques and materials, the actual problem is not only to decrease hazardous effect of SCWAs and GCWAs on the environment and operating personnel but also to recycle solid wastes for obtaining products of industrial and domestic use.

A possibility of SCWA application as sorbents for retaining acid gases and petroleum products, charges for polymer composites, and catalysts for high-temperature (700–900 °C) oxidizing condensation of methane was first demonstrated in [4, 6]. There was clear evidence that catalytic performance of SCWAs in chemical reactions of any type depended on their chemical and phase composition. Chemical and phase composition of SCWAs is a consequence of the nature of both weld materials and welding electrodes, of electrode coating materials and welding conditions [7–17]. As far as we know, there are no data in literature concerning a phase composition of SCWA formed as a result of metal welding by a TsL-11 type electrode (ISO E19.9NbB20). Systematic studies concerning the use of solid wastes for obtaining catalysts for ozone decomposition are also absent there. The only known case is the application of a sludge underflow formed in the process of water purification and enclosing iron oxides for obtaining cement containing catalysts for ozone decomposition at its concentration of *ca.* $2 \cdot 10^4$ mg/m^3 [18].

The aim of the work was to identify a phase composition of the solid component of welding aerosol produced as a result of welding by the TsL-11 type electrode (SCWA-TsL-11) and to study catalytic performance of the latter in the reaction of ozone decomposition at ozone initial concentrations ranging from 1 to 100 mg/m^3.

EXPERIMENTAL

The welding fume fractions of the SCWAs with the aerodynamic diameter ≤ 1 μm formed in the process of metal arc welding by the 3 mm diameter TsL-11 type electrodes (ISO E19.9NbB20) with the carbonate-fluorite electrode coating were selected for the study. Welding was performed under conditions of direct current, reverse polarity, U = 33 V, I = 140–150 A, and the welding speed, V, of 4.5 mm/s). TsL-11 type electrodes produced

from steel wire of Sv-08Kh19N10B grade consisting of Fe (67.0 wt. %), C (0.05–0.10 wt. %), Mn (1.2–1.7 wt. %); Si (0.7 wt. %), Cr (18.5–20.0 wt. %), and Ni (9.0–10.5 wt. %), and having a carbonate-fluorite coating consisting of ferromanganese (5.0 wt. %), marble (54.0 wt. %), derbyshire spar (15.0 wt. %), quartz (9.0 wt. %), ferrosilicium (5.0 wt. %), and ferrotitanium (15.0 wt. %) were used in manual arc welding of high-alloy steels, high alloys, and corrosion-resistant chromium-nickel steels [11].

SCWA-TsL-11 samples were characterized by X-ray diffraction phase analysis, IR spectroscopy, and pH-metry. In addition, they were tested in the reaction of low-temperature ozone decomposition.

The samples were identified based on X-ray diffraction phase analysis data recorded on a Siemens D500 diffractometer (CuK_α radiation, $\lambda = 1.54178$ Å) with a secondary beam graphite monochromator. The phases were identified with the help of ICDD (International Centre for Diffraction Data) PDF-1 databases provided as a part of the Siemens D500 diffractometer software.

Infrared analysis was carried out using a Perkin Elmer FT-IR Spectrometer with resolution of 4 cm^{-1}; pellets consisting of 1 mg of the material under study and 200 mg of KBr were compressed under pressure of 7 tons/cm^2 for 30 s.

The equilibrium pH values measured in an aqueous suspension consisting of SCWA-TsL-11 (0.2 g) and distilled water (20 mL) were used to characterize protolytic properties of surface functional groups of the SCWA. The measuring was carried out by a pH-340 instrument with an ESL 43-07 glass electrode and an EVL 1M3 silver-chlorine electrode at continuous stirring of the suspension at 20 °C.

The catalyst samples (0.5 g) were tested using a gas-flow setup with a fixed bed reactor at 20 °C, relative humidity of 65 %, and the linear velocity (U) of an ozone-air mixture (OAM) equal to 3.2 cm/s. The ozone decomposition was monitored by measuring the final ozone concentration ($C_{O_3}^f$).

In the case of ozone initial concentrations ($C_{O_3}^{in}$) ranging from 10 to 100 mg/m^3, $C_{O_3}^{in}$ and $C_{O_3}^f$ were measured by a Tsyclon-Reverse optical analyzer with the detection limit of 1 mg/m^3 whereas at the initial concentration of 1 mg/m^3, $C_{O_3}^{in}$ and $C_{O_3}^f$ were controlled using a 652ECh04

electrochemical gas analyzer with minimum detectable O_3 concentration of 0.025 mg/m^3.

The reaction rate (W) calculations based on the data of ozone concentration changing after OAM passing through the static bed of the catalyst were made using the following equation:

$$W = \frac{w\left(C_{O_3}^{in} - C_{O_3}^f\right)}{m}, \text{ mol/(g·s)}, \quad (1)$$

where $w = 1.67 \cdot 10^{-2}$ is the OAM volume flow rate, L/s; $C_{O_3}^{in}$ and $C_{O_3}^f$ are the initial and final ozone concentrations in the OAM, mol/L; m is the mass of a catalyst sample, g.

The reaction rate values measured after one minute of OAM passing named as the initial reaction rate, W_{in}, were used to characterize the process.

The reaction rate constant, $k_{1/2}$, was quantified for the half reaction time, $\tau_{1/2}$, i.e. for the moment of time when the degree of ozone decomposition became equal to 50 %, as follows:

$$k_{1/2} = \frac{0.69}{\tau_{1/2}}, \text{ s}^{-1}. \quad (2)$$

The amount of ozone entered into the reaction up to a moment of experiment termination (Q_{exp}, moles of O_3) was calculated as a square of the corresponding ozonogram plotted as a ΔC_{O_3} vs. τ function.

To characterize protective behavior of the SCWA-TsL-11 samples, a period of time required for attaining of $C_{O_3}^f = MPC_{O_3}$, τ_{MPC}, was used.

RESULTS AND DISCUSSION

An X-ray diffraction pattern of the SCWA-TsL-11 sample (Fig. 1) demonstrates a high crystallinity of its individual phases. The most intensive reflections are observed in the range from 28 to 65 °.

The data concerning the phase composition of the SCWA-TsL-11 sample, some characteristics of its X-ray spectrum, i.e. angles of reflection, 2θ, the interplanar spacing (d, Å), both experimental and reference, and also the normalized reflection intensity, I_N, are presented in Table 1. By their help, a probability of formation of various intermetallides, oxides and fluorides of metals, silicate forms, *etc.* can be determined. Taking into consideration the chemical composition of both electrode wire and electrode coating, probable

phases are identified by the help of ICDD PDF-1 File, a part of the diffractometer software. Therefore reflections characterized by $I_N > 20$ are essentially considered, however, sometimes, peaks with $I_N < 20$ must be taken into account when their experimental and reference parameters are in close agreement.
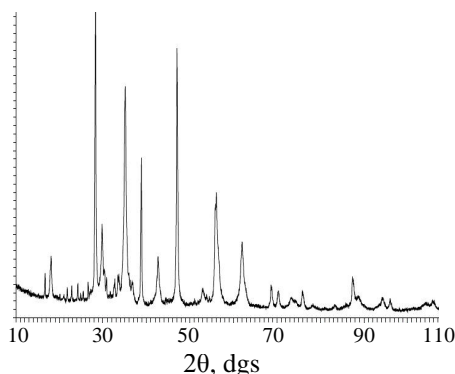

Fig. 1. The X-ray diffraction pattern of the SCWA-TsL-11 sample

Thirteen well-identified phases, such as manganochromite, $(Mn,Fe)(Cr,V)_2O_4$ (ICPDS 31-0630); magnesium silicate, $MgSiO_3$ (ICPDS 11-0273); α-quartz, α-SiO_2 [19]; goethite (red iron ore), Fe_2O_3 [19]; agacansite, β-$Fe_2O_3 \cdot H_2O$ [19]; nickel fluoride, NiF_2 [19]; derbyshire spar, CaF_2 (ICPDS 35-0816); manganese oxide, Mn_3O_4 (ICPDS 13-0162); silicate of calcium and magnesium (mervinite), $Ca_3Mg(SiO_4)_2$ (ICPDS 35-0591); chromium oxide, Cr_2O_3 [19]; nickel oxide NiO [19]; rutile, TiO_2 [19]; and potassium chromate, K_2CrO_4 [12, 19].

Because of superposition of many reflections, the phase identification requires to determine not only the sequence of reflections but also the presence of individual reflections of every phase in the X-ray spectrum. For instance, the most intensive reflection at $2\theta = 28.251°$ (d = 3.156 Å) is a result of superposition of a CaF_2 peak and a $MgSiO_3$ peak with relative intensities according to reference data of 92 and 100 %, respectively. However, these phases have their second individual reflections at $2\theta = 46.999°$ (d = 1.931 Å) for CaF_2 and at $2\theta = 30.804°$ (d = 2900 Å) for $MgSiO_3$. Individual phase parameters also enable the identification of manganochromite having a vanadium impurity (ICPDS 31-0630) in its composition. Though the presence of ferrotitanium in the electrode coating and the fact that the relative intensity of the TiO_2 individual reflection has been found as 100 % [19], it is impossible to draw an unequivocal conclusion about the presence of TiO_2 in the SCWA-TsL-11 because of the absence of

any individual TiO_2 reflection in its X-ray spectrum. The low-level ($I_N = 15$) reflection observed at $2\theta = 54.467°$ (d = 1.683 Å) can be assigned to Cr_2O_3 (1.67 Å), Fe_2O_3 (1.69 Å), and TiO_2 (1.69 Å) or to the superposition of these individual peaks. It should be noted that Tanninen *et al.* [15] also did not reveal TiO_2 in the SCWA they investigated.

Due to the high contents of chromium and nickel in the TsL-11 electrode, Cr_2O_3 и NiO phases are clearly defined in the X-ray spectrum of its SCWA. Besides, chromium as K_2CrO_4 phase can be identified by its high-level ($I_N = 455$) individual reflection at $2\theta = 38.802°$ (d = 2.319 Å). The presence of the sodium (potassium) chromate phase in the SCWA for an E314L type electrode was stated by Tandon *et al.* [12]. Iron oxides are present as goethite, Fe_2O_3, and agacansite, β-$Fe_2O_3 \cdot H_2O$, whereas no magnetite, Fe_3O_4, is identified. The low intensity of Mn_3O_4 reflection is an evidence of a negligible content of this phase in the SCWA-TsL-11 sample. Based on the most intensive peaks, crystallite sizes for some individual phases can be evaluated by the use of the Scherer equation. They are as follows: 89 nm for $(Mn,Fe)(Cr,V)_2O_4$, 83 nm for K_2CrO_4, 67 nm for CaF_2, and 65 nm for $MgSiO_3$. Other intensive reflections are superpositions caused by two or more phases. For example, an intensive reflection ($I_N = 658$) at $2\theta = 35.095°$ (d = 2.555 Å) can be a superposition of peaks assigned to four phases: manganochromite, NiF_2, β-$Fe_2O_3 \cdot H_2O$, and $MgSiO_3$.

IR spectral characteristics. In the region from 4000 to $400 \, cm^{-1}$, the SCWA-TsL-11 sample demonstrates absorption bands corresponding to stretching ($3436 \, cm^{-1}$) and bending ($1637 \, cm^{-1}$) vibrations of water molecules as well as stretching vibrations (1742 and $1381 \, cm^{-1}$) of carbonate-carboxylate groups. The presence of the latter is due to the high-temperature oxidation of carbon monoxide formed as a result of the welding. The spectrum region from 1050 to $410 \, cm^{-1}$ presented in Fig. 2 *a* characterizes stretching and bending vibrations of M–O (M = Cr, Fe) and Fe–OH bonds. For instance, absorption bands at 945 and $886 \, cm^{-1}$ can be assigned to stretching vibrations of Cr–O in chromium oxide [20] although a band at 886 can be attributed also to a stretching vibration of Cr–O in a chromate ion ($\nu = 880 \, cm^{-1}$) [12]. Potassium chromate was revealed by us in a solution obtained after hydrothermal treatment of a SCWA-TsL-11

sample at 60 °C for 2 h. An intensive band at 597 cm^{-1} with shoulders at 615, 559, and 539 cm^{-1} is characteristic of Fe–O bond vibrations in oxides.

It should be noted that exactly this band undergoes a change after the ozonization of a SCWA-TsL-11 sample (Fig. 2 *b*).

Table 1. The results of X-ray phase analysis of the SCWA-TsL-11 sample

Phase	2θ, dgs	I$_N$	experimental	reference	B
(Mn,Fe)(Cr,V)$_2$O$_4$	18.072	122	4.905	4.89	0.2000
	36.685	50	2.448	2.44	0.1400
	56.060	344	1.639	1.63	0.2000
β-Fe$_2$O$_3$·H$_2$O	26.587	42	3.350	3.30	0.2200
	39.290	15	2.291	2.29	0.1200
	46.383	37	1.956	1.96	0.1700
Mn$_3$O$_4$	73.876	21	1.282	1.28	0.1200
	78.794	11	1.214	1.21	0.2200
	89.748	11	1.092	1.09	0.2800
Cr$_2$O$_3$	36.219	53	2.478	2.47	0.1400
	57.519	21	1.601	1.58	0.1800
	109.011	28	0.946	0.946	0.2200
NiO	36.909	24	2.433	2.40	0.1400
	43.298	27	2.088	2.08	0.1750
CaF$_2$	46.999	871	1.932	1.93	0.2400
	68.647	76	1.365	1.365	0.2600
	87.378	113	1.115	1.115	0.3200
NiF$_2$	27.079	21	3.290	3.30	0.2600
	60.973	28	1.518	1.516	0.2000
MgSiO$_3$	27.385	21	3.254	3.240	0.1400
	30.804	50	2.900	2.908	0.2200
K$_2$CrO$_4$	29.249	47	3.051	3.07	0.2200
	30.310	83	2.946	2.96	0.2400
	38.802	455	2.319	2.321	0.2000
(Mn,Fe)(Cr,V)$_2$O$_4$; Mn$_3$O$_4$ (2.98); NiF$_2$ (2.97)	29.787	215	2.997	2.99	0.3600
(Mn,Fe)(Cr,V)$_2$O$_4$; NiF$_2$ (2.53); β-Fe$_2$O$_3$·H$_2$O (2.55); MgSiO$_3$ (2.551)	35.095	658	2.555	2.55	0.3600
(Mn,Fe)(Cr,V)$_2$O$_4$; β-Fe$_2$O$_3$ (2.10)	42.631	147	2.119	2.12	0.2800
(Mn,Fe)(Cr,V)$_2$O$_4$; Fe$_2$O$_3$ (1.485)	61.969	200	1.496	1.50	0.4600
CaF$_2$; MgSiO$_3$ (3.170)	28.251	1000	3.156	3.154	0.1800
CaF$_2$; MgSiO$_3$ (1.642); β-Fe$_2$O$_3$ (1.648)	55.796	325	1.642	1.647	0.2200
CaF$_2$; NiF$_2$ (1.257)	75.827	61	1.254	1.256	0.2600
Mn$_3$O$_4$ (1.62); MgSiO$_3$	56.473	178	1.628	1.621	0.2000
Mn$_3$O$_4$; Fe$_2$O$_3$ (1.485)	62.639	61	1.482	1.48	0.1900

Only one band at 605 cm^{-1} remaining in the spectrum after the ozonization can signify, as it was stated for chromium oxide [20], a change in the coordination number of iron in its oxides.

Protolytic properties. After contacting a SCWA-TsL-11 sample with water for 20 min, pH of this aqueous suspension decreases from 8.85 to 8.55 and does not change after that. A negative value of ΔpH_s (–0.3) indicates that the heterolytic

dissociation of water molecules on Lewis acid sites of the solid surface proceeds in accordance with a basic mechanism E$^+$…OH$^-$/H$^+$.

Catalytic properties. The time dependence of the final ozone concentration obtained for ozone decomposition by SCWA-TsL-11 samples at ozone initial concentrations in the OAM varied from 1 to 100 mg/m^3 is presented in Fig. 3.
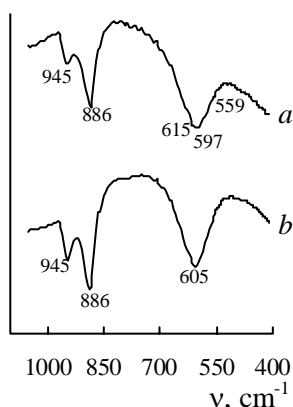
_____

Fig. 2. IR spectra of SCWA-TsL-11 before (*a*) and after (*b*) its ozonization

It is clear that the profiles of kinetic curves depend on $C_{O_3}^{in}$ values. For example, $C_{O_3}^{f}$ is less than 0.1 mg/m^3 (MPC$_{O_3}$) for 140 min at $C_{O_3}^{in}$ =1 mg/m^3 (curve *1*). This subcurve characterizes protective abilities of the SCWA-TsL-11 sample. After that $C_{O_3}^{f}$ slowly increases and attains its stationary level of 0.67 mg/m^3 in 1200 min whereas the ozone concentration at the reactor

outlet increases rapidly up to its initial values at $C_{O_3}^{in}$ of 50 and 100 mg/m^3 (curves *3* and *4*).

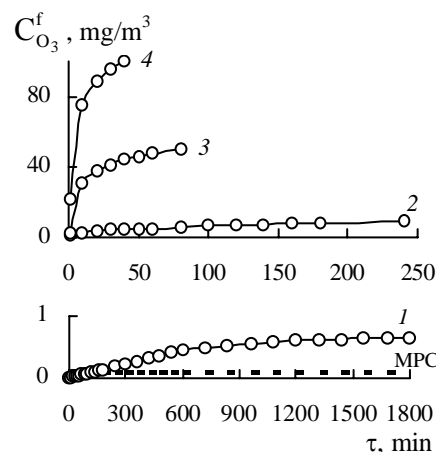Table 2 summarizes some kinetic and stoichiometric parameters of the reaction.

Fig. 3. The time dependence of $C_{O_3}^{f}$ for ozone decomposition by SCWA-TsL-11 samples at different values of $C_{O_3}^{in}$: 1 (*1*), 10 (*2*), 50 (*3*), and 100 mg/m^3 (*4*) (m = 0.5 g, U = 3.2 cm/s, t = 20 °C, w = 1.67·10^{-2} L/s)

Table 2. Effect of $C_{O_3}^{in}$ on kinetic and stoichiometric parameters of the reaction of ozone decomposition over SCWA-TsL-11 samples

$C_{O_3}^{in}$, mg/m^3	W_{in}·10^8, mol/(g·s)	k_1·10^3, s^{-1}	$\tau_{1/2}$, s	$k_{1/2}$·10^4, s^{-1}	Q_{exp}·10^5, moles of O$_3$
1	0.07	-	36000	0.2	1.86
10	0.63	3.6	3600	1.9	1.44
50	3.36	3.8	300	23.0	1.12
100	5.46	3.9	282	24.0	0.91

It can be seen that the initial reaction rate, W_{in}, increases in proportion to $C_{O_3}^{in}$ and the first-order reaction rate constant is changeless except for $C_{O_3}^{in}$ = 1 mg/m^3 when $C_{O_3}^{f}$ = 0. The latter makes impossible the calculation of the reaction rate constant. Other factors characterizing the kinetics of ozone decomposition are the half-reaction time, $\tau_{1/2}$, and the reaction rate constant corresponding to $\tau_{1/2}$, $k_{1/2}$. It is clear that the increase in $C_{O_3}^{in}$ results in a decrease in $\tau_{1/2}$ and in an increase in $k_{1/2}$. Such a variability of $k_{1/2}$ values and a decrease in the amounts of ozone entered the reaction, Q_{exp}, over periods of time equal to $\tau_{1/2}$ are evidence of a chain-radical reaction mechanism.

Taking into account the chemical and phase compositions of SCWA-TsL-11 and according to what is known about ozone decomposition reactions over both oxide catalysts [21] and atmospheric mineral aerosols [22], it can be concluded that the detected phases of manganochromite as well as oxides of iron, chromium, nickel, and manganese are the most probable catalysts of ozone decomposition. Among them, the highest catalytic activity in respect to the reaction under study is characteristic of manganese, nickel, and iron oxides [21]. Contribution of other phases, such as fluorides of calcium and nickel and silicates of magnesium and calcium, to the reaction most likely is minimal. In the case of SCWA-TsL-11, the catalytic performance of the listed active

400

individual oxides can be strengthened by a spinel, $(Mn,Fe)(Cr,V)_2O_4$, which is found not only as an individual phase but also as a combination with manganese and iron oxides (Table 1).

The IR spectrum of the SCWA-TsL-11 sample after its ozonization (Fig. 2 *b*) undergoes a notable change in the range of stretching vibrations of Fe–O bond whereas the bands assigned to vibrations of Cr–O bond in both Cr_2O_3 and chromate ion, CrO_4^{2-}, remain changeless. This can be explained by the facts that Cr_2O_3 is a low-active catalyst [21] and the highest oxidation level of chromium, Cr(VI), does not permit its participation in the reaction with ozone. The equilibrium pH value for the SCWA-TsL-11 aqueous suspension equal to 8.55 also contributes to the reaction of ozone decomposition because alkali or subalkali media promote the reaction [23].

CONCLUSIONS

It has been found that the solid component of welding aerosol formed as a result of high-alloy steel welding by the TsL-11 type electrode (ISO E19.9NbB20) is a crystalline substance containing not less than thirteen phases. Crystallite sizes of individual phases are ranged from 65 to 89 nm.

Manganochromite as well as oxides of iron, manganese, and nickel can decompose ozone at ambient temperatures.

The polyphase composition of the SCWA-TsL-11 has been confirmed by the results of IR spectroscopy. Stretching vibrations of both Cr–O bonds in Cr_2O_3 and chromate and Fe–O and Fe–OH bonds in iron oxides and spinels have been identified. Only one band assigned to vibrations of Fe–O bond alter its position and form after the ozonization of the SCWA-TsL-11 sample.

The first reaction order with respect to ozone has been found at the initial step of the reaction of ozone decomposition over the SCWA-TsL-11 samples at the initial ozone concentration in the OAM ranging from 1 to 100 mg/m^3. A deviation from the first reaction order in the case of half-reaction time is evidence of a chain-radical reaction mechanism. This agrees with the well-known conception of the ozone decomposition over individual metal oxides. The SCWA-TsL-11 sample provides air purification from ozone to the level less than MPC$_{O_3}$ (0.1 mg/m^3) at the initial ozone concentration of 1 mg/m^3 (10 MPC$_{O_3}$) for 140 min.

Фізико-хімічні та каталітичні властивості твердої складової зварювального аерозолю

Т.Л. Ракитська, А.А. Еннан, А.С. Труба, С.А. Киро, В.Я. Волкова

Одеський національний університет імені І.І. Мечникова, хімічний факультет
вул. Дворянська, 2, Одеса, 65082, Україна, truba@onu.edu.ua
Фізико-хімічний інститут захисту навколишнього середовища і людини
вул. Преображенська, 3, Одеса, 65026, Україна

Методами РФА, ІЧ-спектроскопії та рН-метрії охарактеризовані зразки твердої складової зварювального аерозолю, що утворюється під час зварювання сталі електродом ЦЛ-11 (ISO E19.9NbB20). Фази манганохроміту, оксидів заліза, мангану і нікелю обумовлюють каталітичний низькотемпературний розклад озону.

Ключові слова: *зварювальний аерозоль, тверда складова, визначення характеристик, розклад озону, очистка повітря*

Физико-химические и каталитические свойства
твердой составляющей сварочного аэрозоля

Т.Л. Ракитская, А.А. Эннан, А.С. Труба, С.А. Киро, В.Я. Волкова

*Одесский национальный университет имени И.И. Мечникова, химический факультет
ул. Дворянская, 2, Одесса, 65082, Украина, truba@onu.edu.ua
Физико-химический институт защиты окружающей среды и человека
ул. Преображенская, 3, Одесса, 65086, Украина*

Методами РФА, ИК-спектроскопии и pH-метрии охарактеризованы образцы твердой составляющей сварочного аэрозоля, образующегося при сварке стали электродом ЦЛ-11 (ISO E19.9NbB20). Фазы манганохромита, оксидов железа, марганца и никеля обусловливают каталитическое низкотемпературное разложения озона.

Ключевые слова: сварочный аэрозоль, твердая составляющая, определение характеристик, разложение озона, очистка воздуха

REFERENCES

1. *Rakitskaya T.L., Ennan A.A., Bandurko A.Y.* Carbon fibrous materials for a "Snezhok GP-Ozone" type respirator, Avtomat. Svarka, 7 (1995) 62 (in Russian).
2. *Ennan A.A., Rakitskaya T.L., Paina V.Y.* Catalysts for low-temperature carbon monoxide oxidation for purification of welding aerosols, Avtomat. Svarka, 2 (1997) 42 (in Russian).
3. *Ennan A.A., Rakitskaya T.L.* Catching and neutralizing of toxic gaseous substances in welding, Avtomat. Svarka, 1 (2000) 48 (in Russian).
4. *Ennan A.A.* Physicochemical grounds of catching, neutralizing, and recovery of welding aerosols. Environmental Protection, Health, and Safety in Welding: Proc. 1st Int. Sci.-Pract. Conf., Astroprint, Odessa, 2002 P. 10–37 (in Russian).
5. *Ennan A.A., Rakitskaya T.L., Volkova V.Y.* Low-Temperature Catalytic Air Purification from Carbon Monoxide, Astroprint, Odessa, 2005, 191 p. (in Russian).
6. *Shikhaleeva G.N., Chursina O.D., Kutovaya L.M., Shenkevich N.G.* The ways of treatment of the solid component of welding aerosol for obtaining sorbents for environmental purposes. Environmental Protection, Health, and Safety in Welding: Proc. 1st Int. Sci.-Pract. Conf., Astroprint, Odessa, 2002. P. 352–363 (in Russian).
7. *Yavdoshin I.R., Pokhodnya I.K.* Welding aerosol formation in the course of arc fusion welding and the hygienic rating of welding aerosol. Environmental Protection, Health, and Safety in Welding: Proc. 1st Int. Sci.-Pract. Conf., Astroprint, Odessa, 2002. P. 38–56 (in Russian).
8. *Voitkovich V.G., Bezruk L.I., Esaulenko G.B.* Electron microscopic study of the solid component of welding aerosols, Avtomat. Svarka, 6 (1984) 33 (in Russian).
9. *Demenkova L.G.* A welding aerosol and the ways to minimize its effect on the environment. Innovation Techniques and Economics in the Machine-Building Industry: Proc. 3rd Int. Sci.-Pract. Conf., TPU Publ., Tomsk. 2012, P. 194–199.
10. *Ennan A.A., Kiro S.A., Oprya M.V., Vishnyakov V.I.* Particle size distribution of welding fume and its dependency on conditions of shielded metal arc welding, J. Aerosol Sci., 64 (2013) 103.
11. *Oprya M., Kiro S., Worobiec A. et al.* Size distribution and chemical properties of welding fumes of inhalable particles, J. Aerosol Sci., 45 (2012) 50.
12. *Tandon R.K., Payling R., Chenhall B.E. et al.* Applicacion of X-ray photoelectron spectroscopy to the analysis of stainless-steel welding aerosols, Apl. Surface Sci., 20 (1985) 527.
13. *Annoni R., Souza P.S., Petranikova M. et al.* Submerged-arc welding slags:

Characterization and leaching strategies for the removal of aluminum and titanium, J. Hazard. Mater., 244–245 (2013) 335.

14. *Bhamjia I., Preussa M., Threadgillb P.L. et al.* Linear friction welding of AISI 316L stainless steel, Mater. Sci. Eng. A., 528 (2010) 680.

15. *Tanninen V.-P., Hyvarinen H.-K., Grekula A., Kalliomaki P.-L.* Experimental improvements in analysis of aerosol samples by X-ray powder diffraction, J. Aerosol Sci., 16 (1985) 373.

16. *Kumfer B.M., Shinoda K., Jeyadevan B., Kennedy I.M.* Gas-phase flame synthesis and properties of magnetic iron oxide nanoparticles with reduced oxidation state, J. Aerosol Sci., 41 (2010) 257.

17. *Kalliomaki R-L., Aitio A., Lakomaa E.-L., Kalliomaki K.* Kinetics of the metal components of intratracheally instilled mild and stainless steel welding fumes in parts, J. Aerosol Sci., 18 (1987) 737.

18. *Zaloznaya L.A., Tkachenko I.S., Egorova G.V. et al.* Cement-containing catalysts based on iron oxides for ozone decomposition, Vestn. Mosk. Un-ta. Ser. 2. Khimiya, 49 (2008) 183 (in Russian).

19. *Markin L.I.* Reference Book on X-Ray Structure Analysis of Polycrystals, State Publ. House of Phys.-Math. Lit., Moscow, 1961, 863 p. (in Russian).

20. *Davydov A.A.* IR Spectroscopy in Chemistry of Oxide Surface, Nauka, Novosibirsk, 1984, 245 p. (in Russian).

21. *Oyama S.T.* Chemical and catalytic properties of ozone, Catal. Rev. Sci. Eng., 42 (2000) 279.

22. *Michel A.E., Usher C.R., Grassian V.H.* Reactive uptake of ozone on mineral oxides and mineral dusts, Atmospheric Environ., 37 (2003) 3201.

23. *Virdis A., Viola A., Cao G.* A novel kinetic mechanism of aqueous-phase ozone decomposition, Ann. Chim., 85 (1995) 633.